Astron. Astrophys. 351, 201–211 (1999)

ASTRONOMY AND ASTROPHYSICS

Mid–infrared spectral images of planetary nebulae with ISOCAM⋆

P. Persi[1], **D. Cesarsky**[2], **A.R. Marenzi**[1], **A. Preite-Martinez**[1], **D. Rouan**[3], **R. Siebenmorgen**[4], **F. Lacombe**[3], **and D.Tiphene**[3]

[1] Istituto Astrofisica Spaziale, CNR, Area di Ricerca Tor Vergata, Via del Fosso del Cavaliere, 00133 Roma, Italy (persi@saturn.ias.rm.cnr.it)
[2] Institut d'Astronomie Spatiale, Orsay, France
[3] Observatoire de Paris, Meudon, France
[4] ISO Data Centre, ESA Astrophysics Division, Villafranca del Castillo, Spain

Received 27 May 1999 / Accepted 23 August 1999

Abstract. This paper presents the results of ISOCAM–CFV spectral images between 5 and 16.5 μm of the planetary nebulae, NGC 6543, NGC 7027, NGC 6302, NGC 6720, BD+30°3639, VY 2–2, and of the proto–planetary nebula CRL2688. All the nebulae, except VY 2–2 are spatially resolved in the continuum and in the different spectral features. Integrated CVF spectra have been obtained for each nebula, and the line fluxes have been measured for the observed fine–structure ionic lines and infrared emission bands. From the continuum-subtracted images we have analysed the morphologies of the different emission features, and from the deconvolved images and the relative surface brightness distributions, we have derived their sizes.

Key words: ISM: planetary nebulae: general – infrared: ISM: lines and bands

1. Introduction

Planetary Nebulae (PNs) can be easily distinguishable from other celestial objects for their strong emission lines in the optical and infrared spectral regions. In particular the near and mid-IR spectra of PNs are characterized by a variety of fine-structure ionic lines, hydrogen recombination lines, molecular hydrogen emission, and infrared emission bands attributed to fluorescent vibrational transition in polycyclic aromatic hydrocarbon molecules (PAHs) (see for review Allamandola et al. 1989, Puget & Leger 1989). In the past several PNs were observed from the ground in the spectral region 8–13 μm (i.e. Russel et al. 1977, Aitken et al. 1979, Aitken & Roche 1982, Roche & Aitken 1986), from the Kuiper Airborne Observatory (5–8 μm) (Cohen et al. 1989), and between 7.5 and 23 μm with the IRAS low–resolution spectrometer (Pottasch et al. 1986). These observations indicate that at mid-IR wavelengths there are several components which may contribute to the total observed flux. These components are a warm dust continuum, a nebular continuum, ionic emission lines (e.g. Ne, Ar, S, Mg..), a broad silicate feature near 9.7 μm, and infrared emission bands observed in carbon-rich PNs. All these features are not always present at the same time.

With the advent of the mid-IR arrays detectors, a few PNs were imaged at arcsec resolution from the ground in the 8–13 μm region, in order to study the different morphologies of the observed features. Arens et al. (1984), comparing the 10 μm image of NGC 7027 with the radio map obtained at the same resolution, conclude that the warm dust responsible for mid-IR continuum emission is coextensive and well mixed with the gas in the ionized zone, while high resolution mid-infrared images of the low-excitation planetary nebula BD +30°3639 (Hora et al. 1993), have allowed spatial separation of the various spectral emission components, such as the 12.8 μm [Ne II] emission feature, the PAHs emissions and the continuum emission. In particular for this nebula, the 7.7, 8.6 and 11.2 μm emission features, have been found more extended than the continuum and ionized region of the nebula (Bentley et al. 1984). Similarly, Woodward et al. (1989) found in NGC 7027 that the 3.3 μm emission feature extends beyond the ionized region. This suggests a possible destruction of the PAH molecules on the interior edge of the shell from the absorption of strong UV flux from the central star. Therefore, the analysis of distinct morphologies at infrared wavelengths of continuum and emission features, is very important to derive the physical condition within the nebula, and to study the evolution of PNs.

For this reason, we have observed with the Circular Variable Filters (CVFs) of the camera ISOCAM (Cesarsky et al. 1996) on-board of the satellite ISO (Kessler et al. 1996), a sample of seven PNs including the proto-planetary CRL2688, the low-excitation PNs VY 2–2 and BD +30°3639, the young carbon-rich NGC 7027 and NGC 6302, the oxygen-rich PN NGC 6543 and the Ring Nebula NGC 6720. The preliminary results of these observations that constitute the ISOCAM guaranteed time program identified as PPERSI.PPNESPC were discussed by Persi et al. (1997,1999).

In this paper we present for the first time a set of homogeneous spectral images from about 5 to 16 μm of our PNs sam-

Send offprint requests to: P. Persi

⋆ ISO is an ESA project with instruments funded by ESA Member States (especially the PI countries: France, Germany, the Netherlands and the United Kingdom) and with the participation of ISAS and NASA.

Correspondence to: Istituto Astrofisica Spaziale, CNR, Area di Ricerca Tor Vergata, Via del Fosso del Cavaliere, 00133 Roma, Italy

Table 1. Log of the ISOCAM-CVFs observations of Planetary Nebulae.

Nebula	Orbit	Date	LW Spect.Reg. (μm)	SW Spect.Reg. (μm)	Time (sec)
NGC 6543	163	04/27/1996	(5.0–9.0)(9.0–16.5)		7918
NGC 7027	163	04/28/1996	(5.0–9.0)(9.0–16.5)	(3.6–4.6)	6446
CRL2688	163	04/28/1996	(5.0–9.0)(9.0–16.5)	(3.6–4.2)	3577
BD+30°3639	163	04/28/1996	(5.0–9.0)(9.0–16.5)	(3.6–4.2)	4556
NGC 6302	324	10/06/1996	(5.0–9.0)(9.0–16.5)	(3.6–4.2)	11226
NGC 6720	361	11/11/1996	(9.0–16.5)		11130
VY 2–2	547	05/16/1997	(5.0–9.0)(9.0–16.5)	(3.6–4.2)	3770

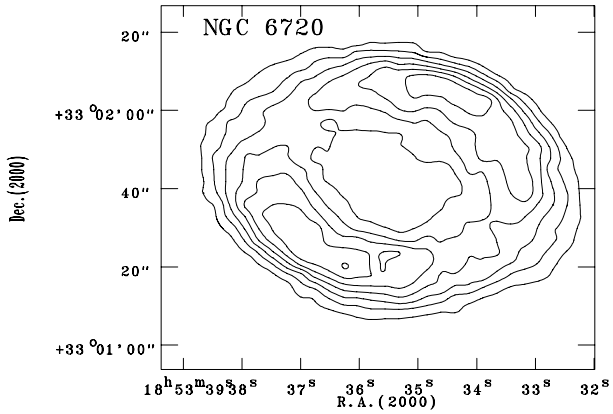

Fig. 1. Averaged contour image at λ_{eff}=12.75 μm of NGC 6720. The lowest contour correspond to 30% of the flux in the peak pixel (9 mJy/pix that is $\sim 5\ \sigma$). Subsequent contours are 40%,50%..100%.

ple. The details of the observations are given in Sect. 2, while in Sect. 3 we analyse the possible extension of the PNs in the mid–IR. The integrated CVF spectra with the measured line intensities are reported in Sect. 4. Finally, in Sect. 5, we discuss separately each PN on the basis of their morphologies observed in the continuum and emission lines.

2. Observations and data reduction

Spectrophotometric images of seven PNs were taken with the CVFs of the mid-infrared camera ISOCAM on-board of the ISO satellite. All the nebulae, except NGC 6720, were observed with 1.5″ pixel scale with the two CVFs in the long -wave channel (LW) of the camera, covering the spectral region between 4.956 and 16.52 μm in 75 spectral points. At each CVF step position 20–40 read-outs were taken with 0.28 or 2.1 s read-out time and gain one or two depending on the brightness of the nebula. At least 30 extra exposures were added for each nebula at the beginning of each scan in order to limit the effect of the transient response of the detector. Sixteen spectral points were also observed with the CVF in the short-wave channel (SW) between 3.64 and 4.32 μm The Ring Nebula (NGC 6720) was observed only between 9.0 and 16.5 μm (38 spectral points) with a pixel field-of-view of 3″, 5.04 s read-out time and gain two.

Table 1 gives the log of the observations including the orbit, the observing date, the total integration time, and the spectral coverage.

The raw data were processed using the CIA software (v3.0) (Ott et al. 1997). The basic data reduction steps are described by Siebenmorgen et al. (1997). Cosmic ray hits were detected and masked using the multiresolution median transform (MMT) method (Starck et al. 1996). The dark current was subtracted using the dark model, and the flat fielding was performed using the CAL-G calibration library flats. Finally the transient effects were corrected with the IAS model (Abergel et al. 1996). At the end of this operation, we obtained a cube of 75 spectral images in the LW channel and 16 images in the SW channel for six nebulae, and 38 spectral images for NGC 6720 in the LW channel.

In order to check the quality of the ISOCAM calibration in CVF mode, we have compared the observed total flux density derived from ground-based images of BD+30°3639 taken with CVF at 10, 11.2, 12.4, 12.8 and 13.2 μm by Hora et al. (1993) with our observations. The agreement is 6%, indicating good quality ISOCAM data.

3. MID–IR extension

Combining the spectral images in the LW channel, we have derived an averaged image at λ_{eff}=12.75 μm for NGC 6720 (Fig. 1), and averaged images at λ_{eff}=10.75 μm for the other six PNs (Fig. 2). NGC 6720 (The Ring Nebula), shows a ring structure extending 66″ × 78″, very similar to that observed in the optical emission line H_α and [N II] line by Guerrero & Manchado (1997). Different sizes and morphologies are observed in the other PNs of our sample (see Fig. 2).

VY 2–2 appears unresolved at our spatial resolution of 3.42″ (FWHM of the theoretical point-spread-function (PSF) at 10.5 μm), while BD+30°3639, and the proto-planetary nebula CRL2688 are extremely compact. NGC 7027 and NGC 6543 show an ellipsoidal morphology in the mid–IR with a size of 9″ × 11″ and 16.5″ × 19.5″ respectively. The central part of the bipolar nebula NGC 6302 is extended ($\sim$ 11″) in the N–S direction in agreement with the mid–IR map of Lester & Dinerstein (1984).

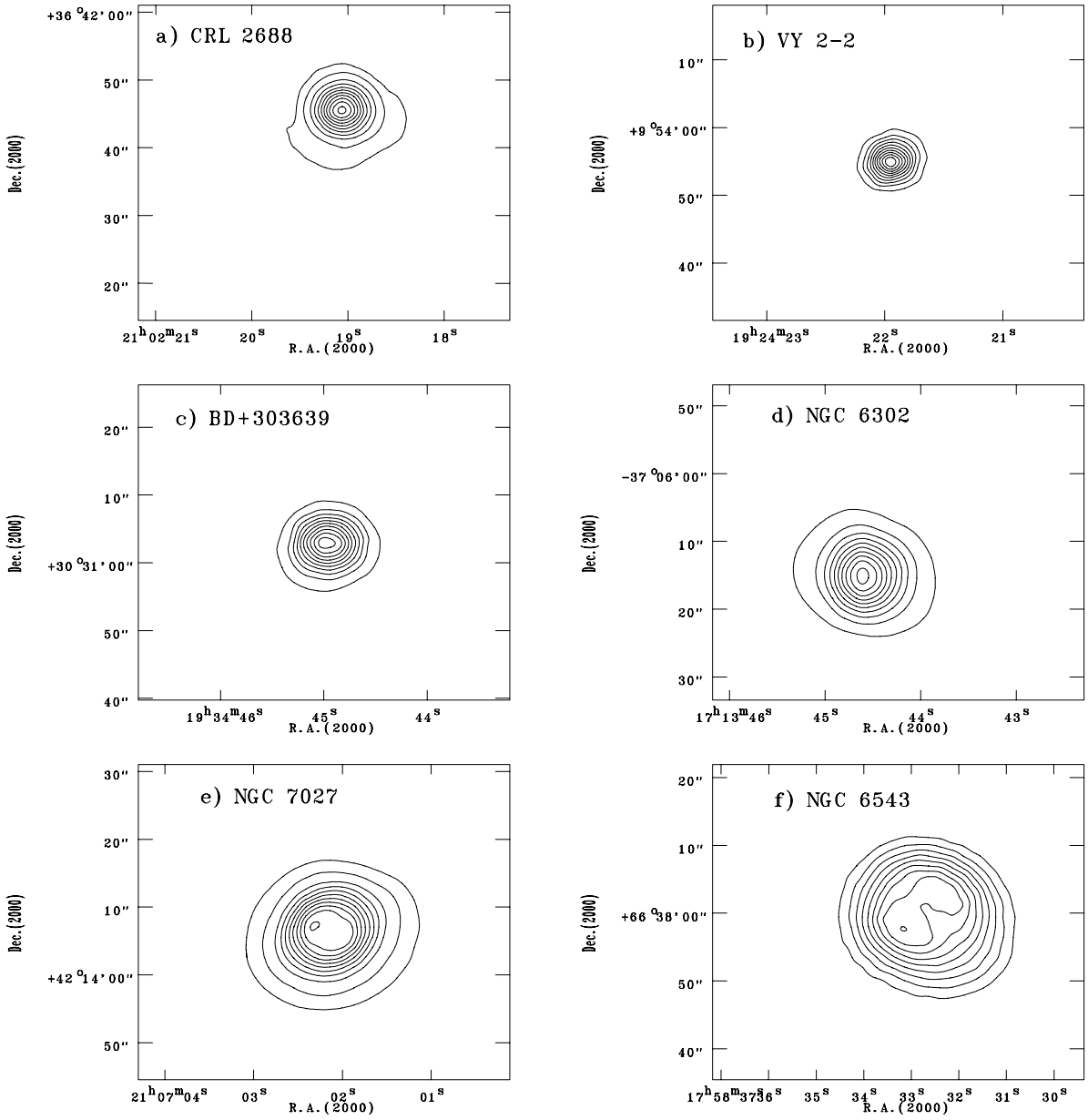

Fig. 2a–f. Averaged contour images of PNs at λ_{eff}= 10.75 μm. The lowest contour level correspond to 10% of the flux in the peak pixel, and in all cases the minimum contour level is $\geq 5\sigma$. Subsequent contours represent 20%,30%..100% **a** CRL2688: minimum level 1114 mJy/pix. **b** VY 2–2: minimum level 68.4 mJy/pix. **c** BD+30°3639: minimum level 196.8 mJy/pix. **d** NGC 6302: minimum level 58.4 mJy/pix. **e** NGC 7027: minimum level 210.7 mJy/pix. **f** NGC 6543: minimum level 19.9 mJy/pix.

4. CVF spectra

Integrating over the whole nebula, we have obtained the CVF spectrum between 9 and 16.5 μm of NGC 6720 (Fig. 3), and the CVF spectra between 5 and 16.5 μm of NGC 7027, NGC 6302, NGC 6543, BD+30°3639, VY 2–2 and CRL2688 (Fig. 4).

The nebulae under study show a wide variety of spectra, from those containing high excitation fine-structure ionic lines such as [Ne V], [Ne VI] and [Mg V] and the PAH emission features at 6.2, 7.7 8.6, and 11.3 μm (NGC 6302 and NGC 7027), to those dominated by a strong continuum emission without emission lines (CRL2688) or with the presence of the silicate band in emission at 9.7 μm (VY2–2). The extended PNs NGC 6543 and NGC 6720, have a similar spectrum dominated by the presence of the strong [Ne III] emission line. We have identified in the Ring Nebula the H_2 (S(3) (0,0)) line at 9.66 μm, with a flux of 2.7 10^{-12} erg cm^{-2} s^{-1}, while the observed emission feature at 7.42 μm in NGC 6543 could be identified with H I (6–5) line.

The measured integrated fluxes of the fine-structure lines identified in our PNs are listed in Table 2.

The central part of the bipolar nebula NGC 6302 has been also observed with the ISO Short-Wavelength Spectrometer (SWS) by Pottasch & Beintema (1997). The agreement between

Table 2. Integrated line fluxes (10^{-10} erg cm^{-2} s^{-1}).

Nebula	Brα (4.05 μm)	[Mg V] (5.61 μm)	[Ar II] (6.98 μm)	[Ne VI] (7.65 μm)	[ArIII] (8.99 μm)	[S IV] (10.51 μm)	[Ne II] (12.81 μm)	[Ne V] (14.32 μm)	[Ne III] (15.56 μm)
NGC 6543			0.02		0.99	2.15	0.23		8.47
NGC 7027	0.66	3.18	1.80	21.61	0.80	6.37	1.77	14.99	11.32
BD+30°3639	0.15		0.93				2.32		
NGC 6302	0.08	1.13	0.63	5.29	1.17	0.90	1.38	7.52	5.33
NGC 6720						0.29	0.13	0.07	2.60
VY 2–2	0.02						0.11		0.28

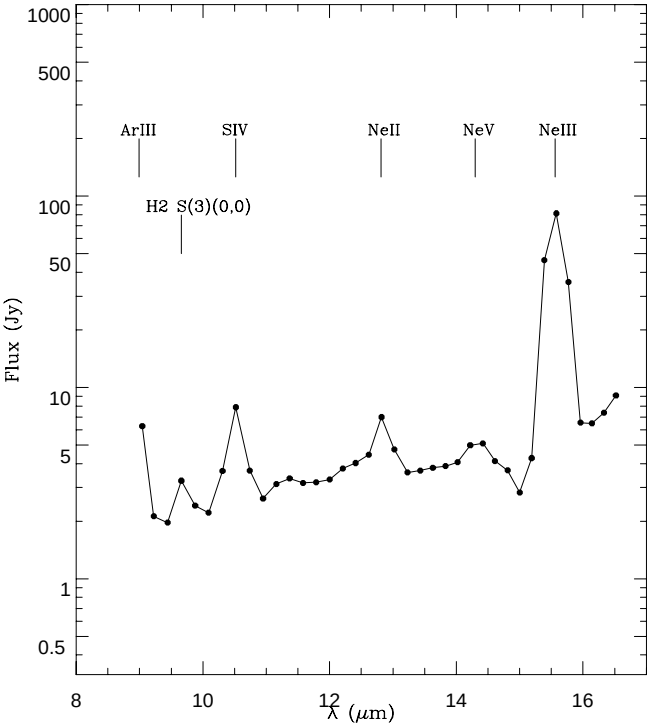

Fig. 3. CVF spectrum of NGC 6720. The spectrum has been measured over an area of 78 square arcsec. The statistical errors are $\leq 3\%$.

our measured fluxes of the neon and sulfur lines of Table 2, with those obtained with the SWS is within 20–25% that represents probably the combined uncertainty of the measurements.

In Table 3 are given the fluxes of infrared emission bands at 6.2, 7.7, 8.6 and 11.3 μm that are present in the CVF spectra of NGC 7027, NGC 6302 and BD+30°3639 (Fig. 4) and ascribed to PAHs. The 7.7 μm emission feature in NGC 7027 and NGC 6302 is blended with the strong [Ne VI] line and therefore their fluxes are not given. The infrared emission bands have been found in a variety of objects such as planetary nebulae, HII regions, reflection nebulae around early type stars, and some external galaxies, but with different average relative intensities with respect to the 7.7 μm band (Cohen et al. 1989). The measured ratio I(6.2)/I(7.7)=0.26 of BD+30°3639 is anomalous with respect to that derived for PNs by Cohen et al. (1989) (0.41), but very similar to that observed with the ISOPHOT low-resolution spectrometer by Mattila et al. (1996) in the diffuse emission of the galactic disk. On the other hand, BD+30°3639 is the only

Table 3. Integrated line fluxes (10^{-10} erg cm^{-2} s^{-1}) of the infrared bands.

Nebula	6.2 μm	7.7 μm	8.6 μm	11.3 μm
NGC 7027	6.54	–	3.78	16.94
NGC 6302	0.51	–	0.28	0.42
BD+30°3639	1.73	6.64	2.37	1.95

Table 4. Colour temperatures and continuum flux densities at 5.2 and 16.2 μm

Nebula	$I_{5.2}$ (Jy)	$I_{16.2}$ (Jy)	$T_{[5.2-16.2]}$ K
NGC 6543	0.25	20.7	152
NGC 7027	14.25	489.5	164
BD+30°3639	3.38	102.89	165
NGC 6302	1.59	57.2	163
VY 2–2	0.27	36.1	146
CRL 2688	8.49	1510.8	143

nebula in our sample in which this ratio has been measured. In addition the ratio I(11.3)/I(6.2) for the three PNs seems to be correlated with the gas phase C/O ratio. Finally, although the CVF spectrum of the carbon-rich post-AGB object CRL 2688 is dominated by a strong continuum, we confirm the presence of the 6.2 and 8.6 μm infrared bands observed by Buss et al. (1993) with KAO.

Assuming that the observed continuum emission of our PNs is due to dust grains with a power law emissivity $Q_\lambda \propto \lambda^{-2}$, from the continuum fluxes at 5.2 and 16.2 μm we have computed the colour temperatures using the relationship:

$$\frac{I_{16.2}}{I_{5.2}} = 3.51\ 10^{-4}\,\frac{e^{2767/T}-1}{e^{886.5/T}-1}$$

The derived colour temperatures and the space integrated continuum fluxes at 5.2 and 16.2 μm are reported in Table 4.

The estimated error in the computed colour temperatures is $\sim 10\%$. It is interesting to note that although our sample contains nebulae at different evolutionary stages, from very young to very diffuse, and with different excitations, the measured color temperature is roughly constant.

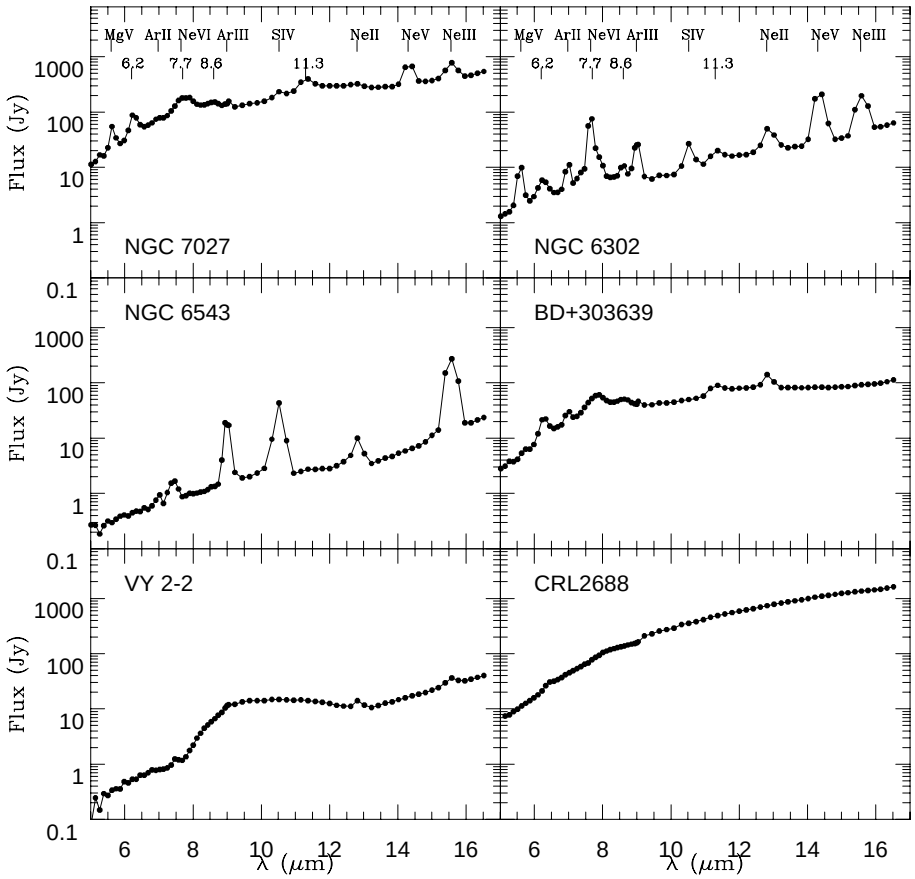

Fig. 4. CVF spectra between 5 and 16.5 μm of PNs. The spectra of NGC 7027, NGC 6302 and NGC 6543 have been measured over an area of 25 square arcsec, while the spectra of BD+30°3639, VY2–2 and CRL2688 have been measured over an area of 15 square arcsec. The statistical errors are typically $\leq 3\%$.

5. Spectral images

For each emission feature present in the CVF spectra of Figs. 3 and 4, we have derived the continuum images from the data cubes. In this section we present the analysis of the continuum-subtracted images. The Lucy-Richardson spatial resolution enhancement algorithm (Richardson 1972, Lucy 1974) has been used to deconvolve the images. We used the theoretical CVF point-spread-function taken in the CIA library. Applying this treatment to our images, all with high signal–to–noise ratio, a spatial resolution of $\sim$1.7″ can be obtained.

5.1. CRL 2688 and VY 2–2

CRL 2688 (Egg Nebula) is a bipolar proto-planetary nebula. As seen in the previous section, the CVF spectrum (see Fig. 4) shows a hint of the infrared bands at 6.2 and 8.6 μm. As the continuum underlying these features is very strong it is impossible to derive the continuum-subtracted images. The averaged contour image of Fig. 2a shows an elongated N–S structure similar to that observed in the 10 μm image taken with CVF at higher spatial resolution by Hora et al. (1996). Their measured flux density at 10 μm with an aperture of 8 ″ is roughly 30% higher of our integrated flux density. This could indicate a variability in the mid-IR on time scale of years as also noted by Hora et al. (1996).

The spectral images centered on the [Ne II] and [Ne III] lines as well as the continuum image (Fig. 2b) of the low-excitation nebula VY 2–2 appear point-like at our spatial resolution. This result is in agreement with the Hα image taken with HST WFPC2 by Sahai & Trauger (1998) that indicates an averaged size of the ionized nebula of 0.6″.

5.2. BD+30°3639

In Fig. 5 we report the continuum-subtracted images of [Ar II] and [Ne II] emission lines and of the infrared bands at 6.2 and 11.3 μm of the low excitation PN BD+30°3639. All the images are spatially resolved with a larger extension in the E–W direction. No significant difference in the spatial extent of infrared bands, continuum emission and the ionic line [Ar II] is observed. This is in agreement with the two dust component model proposed by Siebenmorgen & Krugel (1992). This model predicts for BD+30°3639 a radial profile almost constant with wavelengths in the mid-infrared (Siebenmorgen et al. 1994). The morphology of the [Ne II] line with a ringlike structure is similar to that observed in the Hα HST image reported by Sahai & Trauger (1998). The deconvolved contour image illustrated in Fig. 6 shows essentially the same structure of the original frame with an effective size of 6.2 ″ $\times$ 5.7″ consistent with that obtained from the [Ne II] image by Hora et al. (1993). From our analysis, we cannot confirm the results found by Bentley et al. (1984) and by Hora et al. (1993) in which the emission bands at

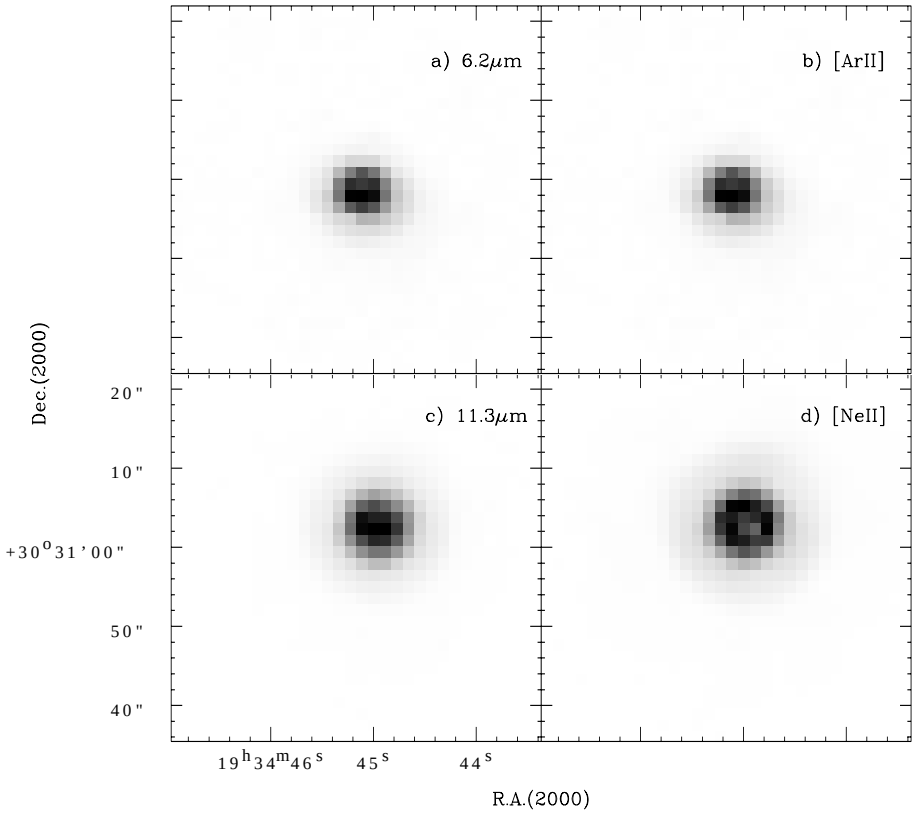

Fig. 5a–d. Continuum–subtracted images of BD+30°3639. **a** 6.2 μm, **b** [Ar II], **c** 11.3 μm, **d** [Ne II]. The gray scale is linear in counts per pixel.

7.7, 8.6 and 11.3 μm are more extended than the continuum and ionized regions. In BD+30°3639, we found that the emitting dust is well mixed with the ionized gas, and that the carriers of the infrared bands (PAHs) are present within the ionized zone.

5.3. NGC 7027

The continuum–subtracted images of the infrared bands at 6.2 and 11.3 μm and of the high and intermediate excitation ionic lines [Mg V], [Ne V], [S IV], and [Ne III] are given in Fig. 7. The 6.2 and 11.3 μm continuum-subtracted images present an elliptical morphology with two bright lobes aligned along the minor axis of the nebula (PA=60°). A similar morphology is observed at 3.3 μm, in the hydrogen recombination lines Brα and Brγ, and in the radio continuum (Woodward et al. 1989, Latter et al. 1995, Basart & Daub 1987). More compact and with a circular shape appears the emission of the high–excitation lines. From the deconvolved images, we have computed the FWHM sizes along the minor axis (PA=60°) and major axis (PA=150°) of the nebula (see Table 5). Comparing these values, we found that the 6.2 and 11.3 μm emission features are spatially more extended than the ionic lines that trace the distribution of ionized gas, and of the continuum emission at 9.8 μm. This is well illustrated in Fig. 8, where we show the normalized surface brightness distributions of the 6.2 μm emission feature, the 9.8 μm continuum emission and the [Mg V] line, along the minor axis of NGC 7027.

Our results are in agreement with the near-IR spectroscopic observations of Woodward et al. (1989), and the mid-IR images of Arens et al. (1984). These observations support the hypothesis of a two–component dust model, with PAHs possibly destroyed by UV flux of the central star on the inner side of the nebula dominated by the ionized region.

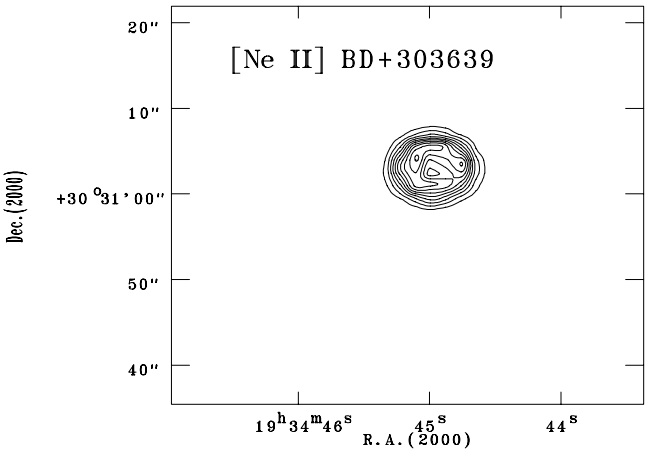

Fig. 6. Contour levels of the deconvolved [Ne II] image of BD+30°3639. The lowest contour correspond to 10% of the flux in the peak pixel. Subsequent contours are 20%,30%..100%

5.4. NGC 6302

Mid–IR spectral images of the high–excitation nebula NGC 6302 are shown in Fig. 9. Our images cover only the central part of the nebula (48×48 sq. arcsec). In fact, the image taken

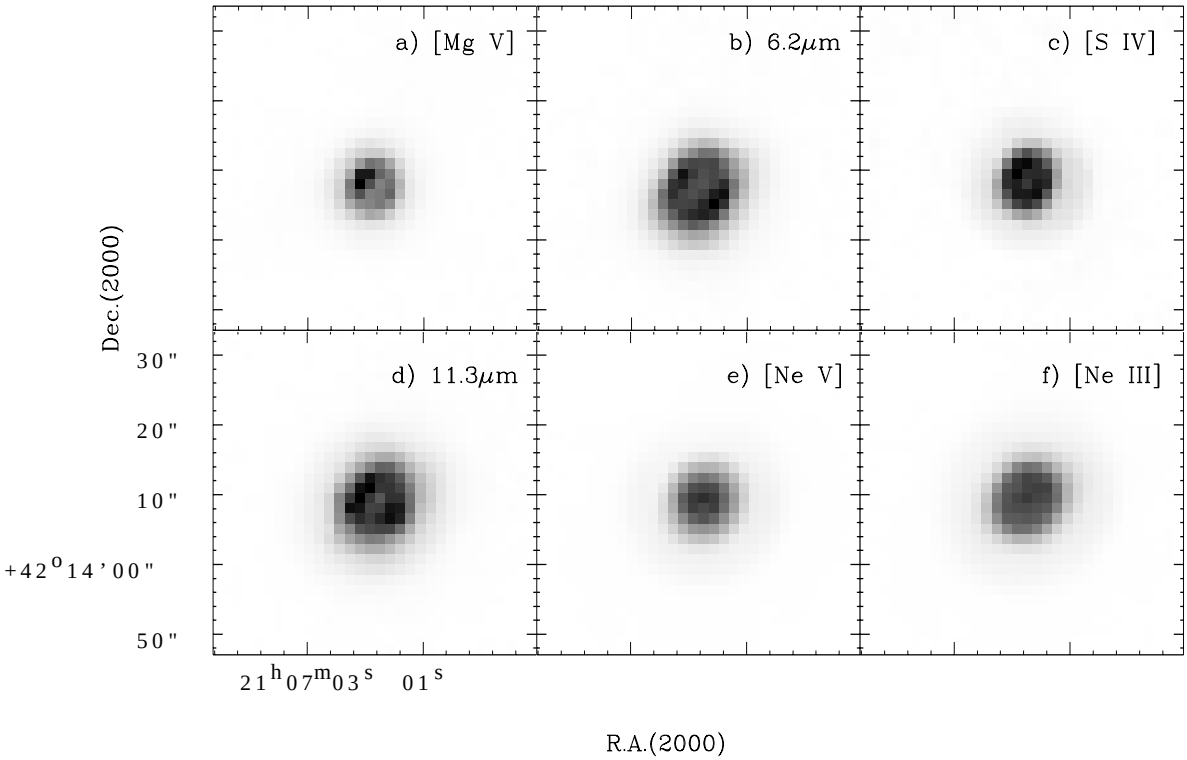

Fig. 7a–f. Continuum–subtracted images of NGC 7027. **a** [Mg V], **b** 6.2 μm, **c** [S IV] **d** 11.3 μm, **e** [Ne V] and **f** [Ne III]. The gray scale is linear in counts per pixel and darker means more intense.

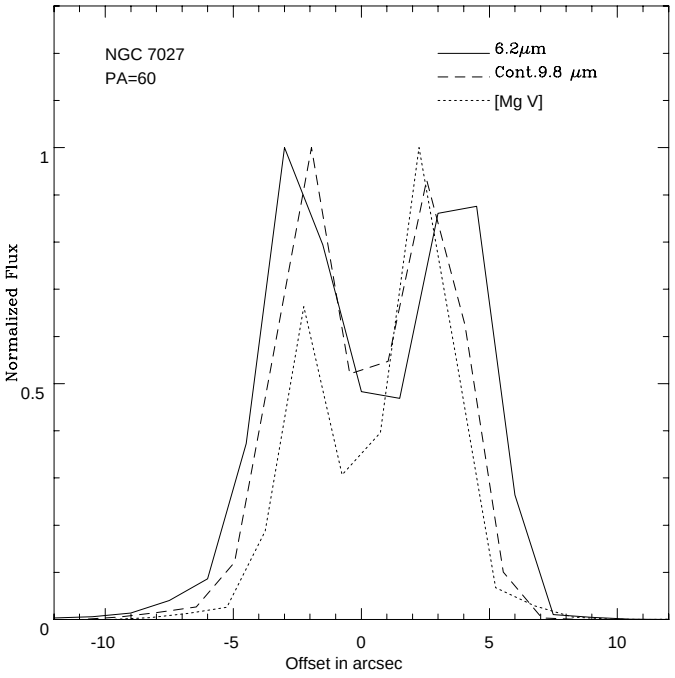

Fig. 8. Surface brightness distributions of some selected emission features and continuum emission along the minor axis (PA=60°) of NGC 7027. Profiles have been normalized to the peaks.

in the light of [Ne V] 3426 Å by Bohigas (1998) has shown that the excited plasma extends $\sim 45''$ at both sides of a central lane bisecting the nebula.

Distinct morphologies are evident in the PAH emission features and in the fine–structure ionic lines. The 6.2 and 11.3 μm emission bands show a double–peaked emission along the N–S direction. The intensity ratio I(11.3)/I(6.2) varies by a factor 4 from the north to the south of the nebula, with the north dominated by the 6.2 μm emission. In the PAH model (Allamandola et al. 1989) the 6.2 μm band is due to the C–C stretching vibration, while the 11.3 μm band is due to the C–H out-of–plane bending vibration. Therefore, this result could imply a composition change, or a dehydrogenation mechanism in the PAH population from north to south. In addition the infrared bands are spatially more extended than the continuum emission as shown in the surface brightness distributions of Fig. 10 (upper panel) obtained from the deconvolved images.

The continuum–subtracted images centered on the [S IV] and on the [Ne III] lines are slightly elongated along position angle $\sim 50°$, while the emission of the higher excitation lines such as [Ne V], [Ne VI] and [Mg V] appear rounder and more compact (see the lower panel of Fig. 10).

5.5. NGC 6543

An elliptical ring morphology is observed in the continuum–subtracted images centered on the fine-structure ionic lines of

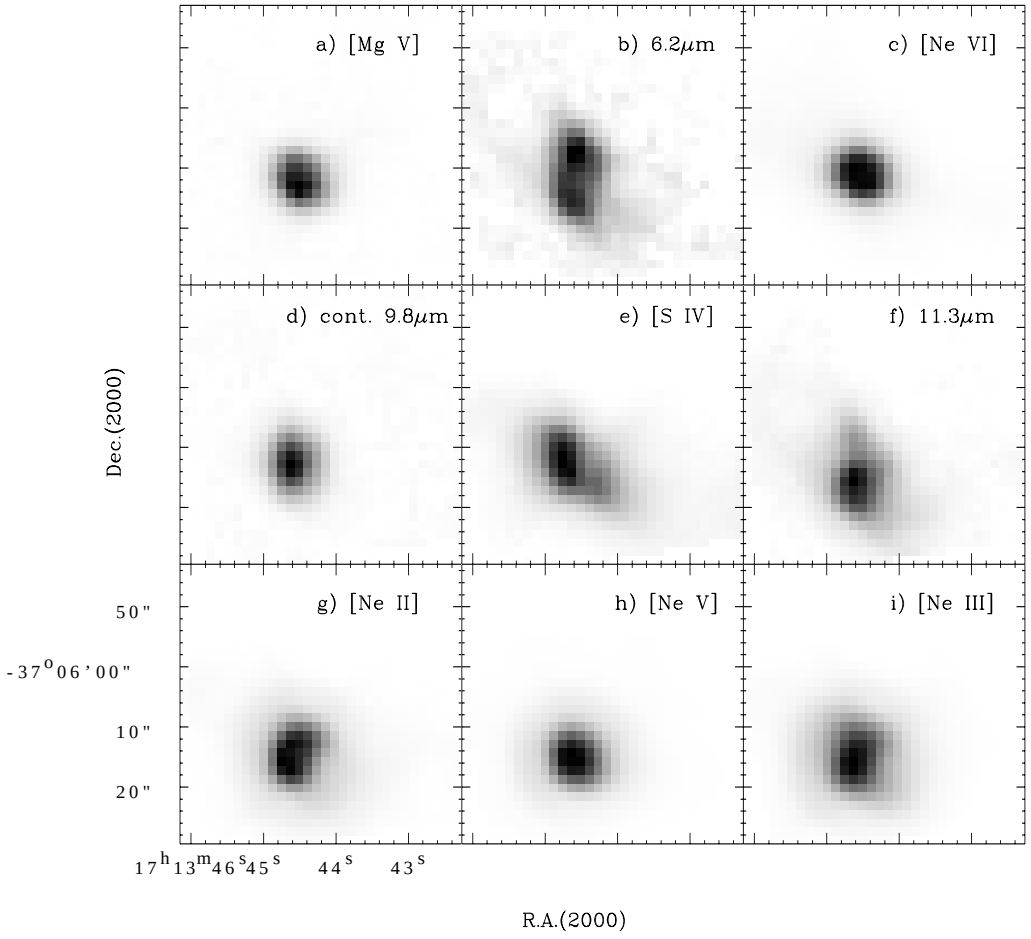

Fig. 9a–i. Continuum-subtracted images of NGC 6302. **a** [Mg V], **b** 6.2 μm, **c** [Ne VI] **d** cont.9.8 μm, **e** [S IV], **f** 11.3 μm, **g** [Ne II], **h** [Ne V], and **i** [Ne III]. The gray scale is linear in counts per pixel and darker means more intense.

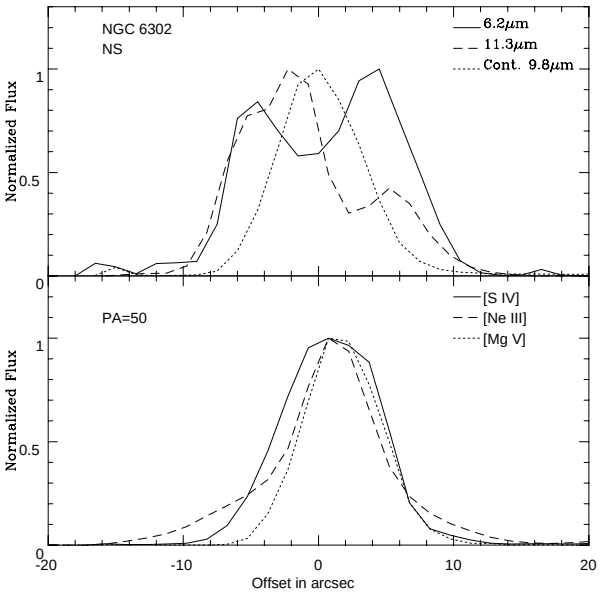

Fig. 10. Surface brightness distributions of some selected emission features and continuum emission of NGC 6302; upper panel: profiles in declination with south at the left; lower panel: profiles along the position angle PA=50°. All the profiles have been mormalized to the peaks.

the oxigen-rich nebula NGC 6543 (see Fig. 11). The minor axis of the nebula is at position angle $\sim 130°$.

We have derived the sizes of the nebula in the different spectral lines and in the continuum emission, using the deconvolved images. The measured FWHM sizes are reported in Table 6.

The morphologies and sizes relative to the [Ar III], [S IV] and [Ne III] lines that have similar ionization potentials, are nearly identical one to each other, as it is also evident from the surface brightness distributions along the minor axis of Fig. 12. For [Ne II] and [S IV], the ratio of the peak surface brightness in the ring to that at the nebular centre is about 1.7–2.0.

Finally, the 9.8 μm continuum ascribed to warm dust grain emission shows a double peaked emission situated inside the ionized region.

5.6. NGC 6720

In Fig. 13 we show the mid–IR spectral images of NGC 6720 (The Ring Nebula). While the [Ne II] and [Ne III] are localized in an ellipsoidal ring structure, the [Ne V] emission fills the center inside the bright shell.

The ionization stratification in the nebula is well illustrated in Fig. 14 by the surface brightness profiles in the [S IV], [Ne III] and [Ne V] lines along the minor axis of the nebula at PA

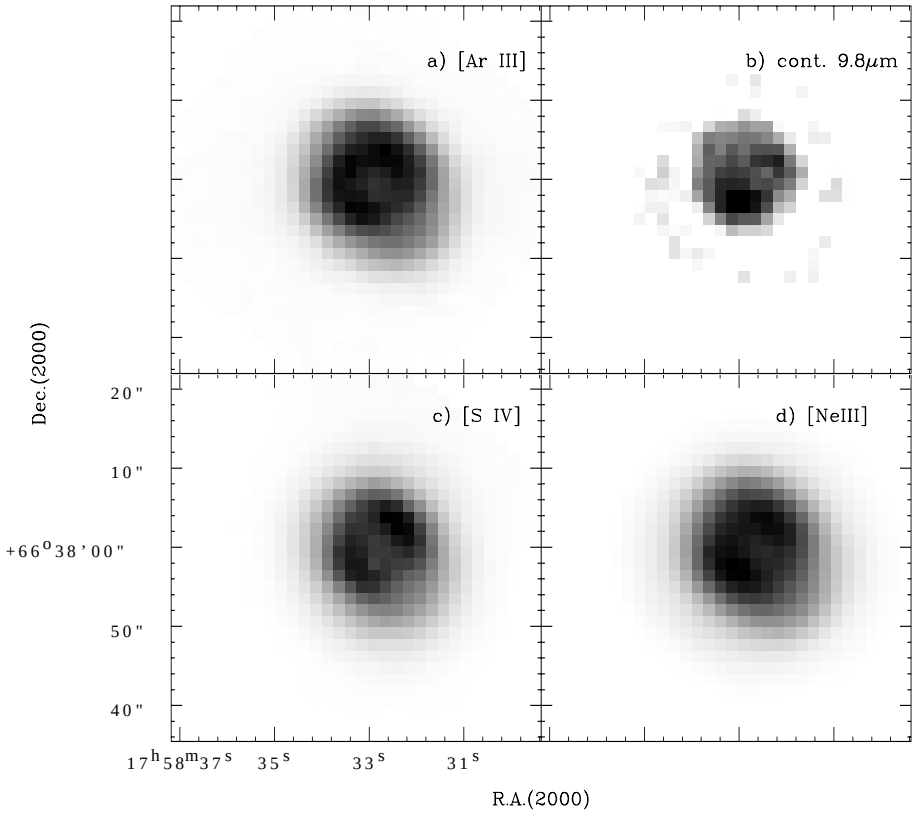

Fig. 11a–d. Continuum–subtracted images of NGC 6543. **a** [Ar III], **b** Continuum 9.8 μm, **c** [S IV] **d** [Ne III]. The gray scale is linear in counts per pixel and darker means more intense.

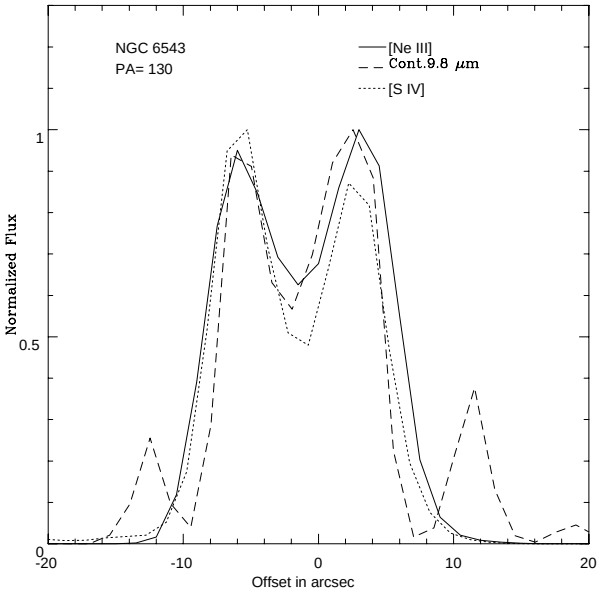

Fig. 12. Surface brightness distributions of some selected emission features and continuum emission of NGC 6543. Profiles are along the position angle PA=130°, and have been mormalized to the peaks.

$\sim$145°. The [S IV] and [Ne III] lines reach their peak emission at $\sim$ 15″ and 25″ from the central star, respectively.

In addition, the ratio of peak to central emission, I_{peak}/I_{center} is 6.4 for [Ne III] and 3.7 for [S IV], suggesting that this ratio depends strongly on the stage of ionization.

Table 5. FWHM sizes of NGC 7027

Line	PA=60° ″	PA=150° ″
Mg V	6.3	6.3
6.2 μm	9.3	10.4
9.8 μm Cont.	7.5	8.0
S IV	6.2	6.9
11.3 μm	8.9	9.7
Ne V	6.1	6.6
Ne III	7.1	8.4

Table 6. FWHM sizes of NGC 6543

Line	PA=130° ″	PA=40° ″
Ar III	13.7	15.2
9.8 μm Cont.	11.9	11.0
S IV	13.0	13.7
Ne III	13.5	15.2

Table 7. FWHM sizes of NGC 6720

Line	PA=145° ″	PA=55° ″
S IV	48	51
Ne II	69	78
Ne V	19	20
Ne III	63	72

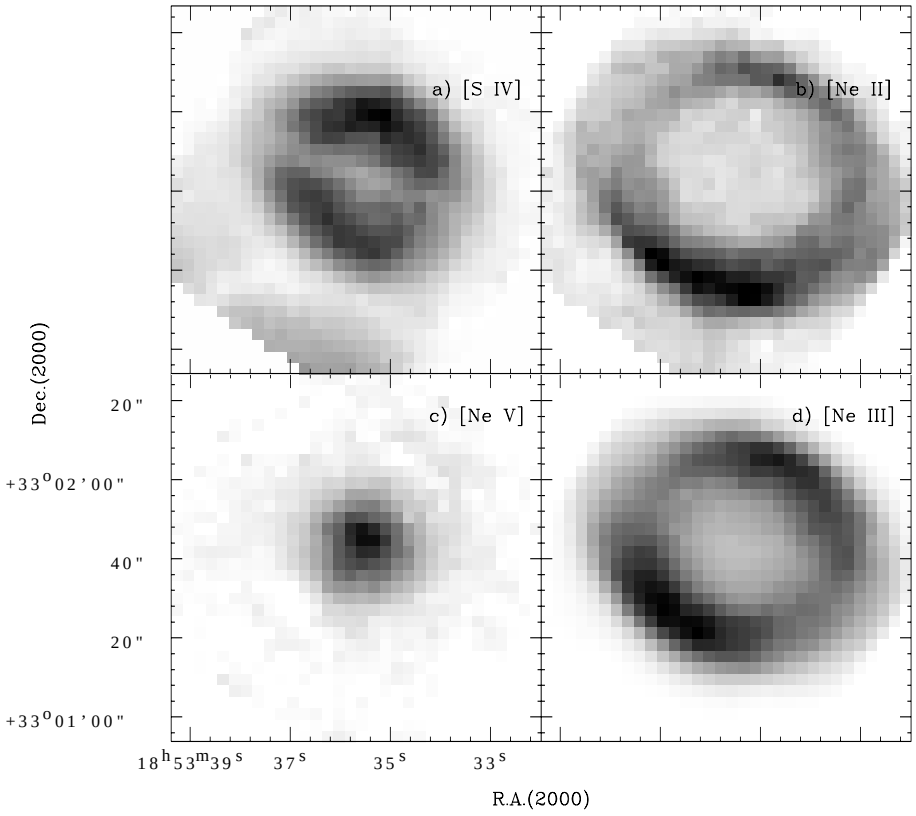

Fig. 13a–d. Continuum–subtracted images of NGC 6720. **a** [S IV], **b** [Ne II], **c** [Ne V] **d** [Ne III]. The gray scale is linear in counts per pixel and darker means more intense.

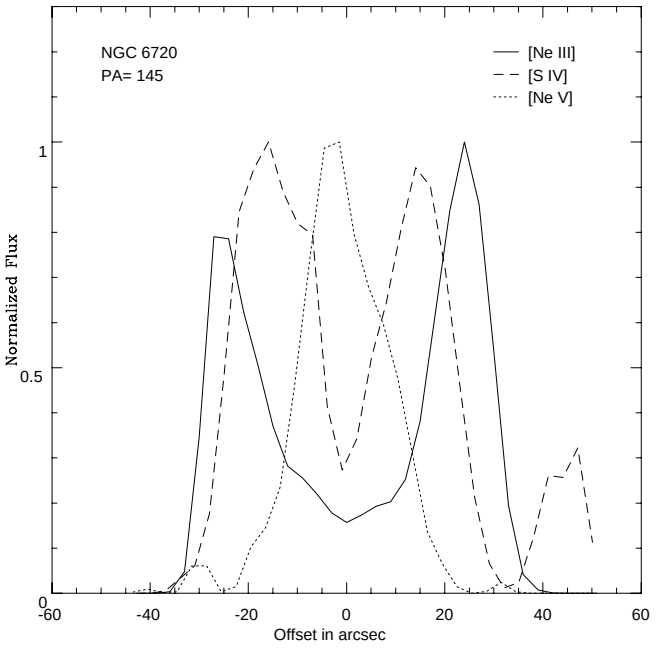

Fig. 14. Surface brightness distributions of some selected emission features and continuum emission of NGC 6720. Profiles are along the position angle PA=150°, and have been mormalized to the peaks.

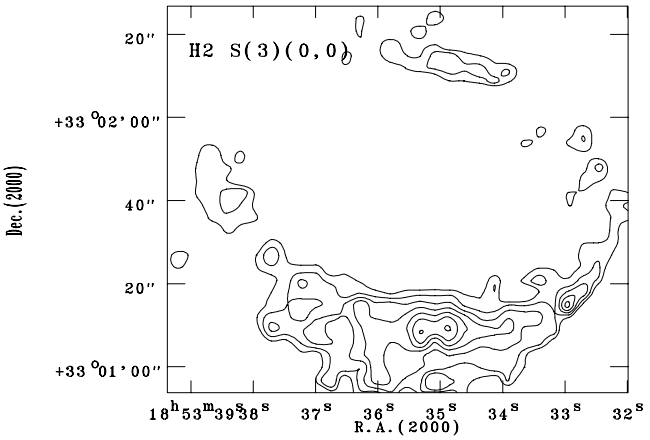

Fig. 15. Contour levels of the H_2 S(3)(0,0) line of NGC 6720. The lowest contour correspond to 10% of the flux in the peak pixel. Subsequent contours are 20%,30%..100%.

The measured sizes obtained from the deconvolved spectral images are reported in Table 7.

The distribution of the molecular hydrogen line S(3)(0,0) identified in NGC 6720, exibits a clumplike distribution, and extends well beyond the bright ring (Fig. 15). This image is very similar to that obtained with the narrow band filter centered at 2.122 μm (H_2 v=1–0 S(1)) by Latter et al. (1995). A detailed comparison between these two H_2 images will be presented elsewhere.

6. Conclusions

ISOCAM with its high sensitivity and moderate spectral and spatial resolution, has allowed for the first time a collection of a set of homogeneous spectral images between 5 and 16.5 μm of

a selected sample of PNs. All the nebulae, except VY2–2, are spatially resolved in the continuum emission and in the different emission features observed in the CVF spectra. Their measured sizes have been obtained from the deconvolved images obtained using the Lucy–Richardson method, and are reported in Tables 5, 6 and 7. In addition the measured integrated line fluxes for the ionic lines and infrared bands are given in Tables 2 and 3.

From a comparison of the continuum–subtracted images relative to the fine– structure ionic lines, infrared emission bands, and continuum emission the following conclusions can be given for each nebula:

1) BD+30°3639 does not show a significant difference in the spatial extent at different wavelengths in the mid-IR, supporting the dust model of Siebenmorgen et al. (1994) in which three different populations of dust particles are co-extensive.
2) The morphologies observed in NGC 7027 of the high excitation [Mg V] line and of the 6.2 and 11.3 μm emission bands are different. The PAHs show an elliptical morphology with two bright lobes aligned along the minor axis of the nebula, while more compact and with a circular shape appear the emission of the high-excitation lines. In addition the PAHs are spatially more extended than the ionic lines that trace the distribution of ionized gas, and of the continuum emission. These results are in agreement with previous near and mid-IR spectral images of Woodward et al. (1989) and Arens et al. (1984).
3) The continuum emission image of the bipolar PN NGC 6302 confirms the presence of a disk at the center of the nebula. A double–peaked emission oriented in the same direction as the continuum emission and spatially more extended, is observed in the infrared bands at 6.2 and 11.3 μm (see Fig. 10).
4) Elliptical ring morphologies are observed in the spectral line images of the oxygen-rich nebulae NGC 6543. The [Ar III], [S IV], and [Ne III] lines with similar ionization potential are nearly identical to each other (Fig. 12). We have derived minor axis of NGC 6543 at a position angle PA$\sim$130°.
5) The Ring Nebula (NGC 6720) is the most extended nebula in our sample. The [Ne II] and [Ne III] spectral images are very similar to that observed in the optical line Hα. While the [Ne II] and [Ne III] emission is mostly localized in in an ellipsoidal ring structure, the [Ne V] emission fills the center inside the bright shell. Finally a clumplike distribution extending well beyond the bright ring is observed in the molecular hydrogen emission (Fig. 15). A more detailed analysis of the ionization structure of these PNs and in particular of the Ring Nebula with a photo–ionization code is in progress, and will be presented in a forthcoming paper.

Acknowledgements. The ISOCAM data presented in this paper were analysed using 'CIA', a joint development by the ESA Astrophysics Division and the ISOCAM Consortium. The ISOCAM Consortium is led by the ISOCAM PI, C.Cesarsky, Direction des Sciences de la Matiere, C.E.A., France.

References

Abergel A., Bernard J.P., Boulanger F., et al., 1996, A&A 315,L329
Aitken D.K., Roche P.F., 1982, MNRAS 200,217
Aitken D.K., Roche P.F., Spenser P.M., Jones B., 1979, ApJ 233,925
Allamandola L.J., Tielens A.G.G.M., Barker J.R., 1989, ApJS 71,733
Arens J.F., Lamb G.M, Peck M.C., et al., 1984, ApJ 279,685
Basart J.P., Daub C.T., 1987, ApJ 317,,412
Bentley A.F., Hackwell J.A., Grasdalen G.L., Gehrz R.D., 1984, ApJ 278,,665
Bohigas J., 1998, Rev. Mex. Astr. Astrofis. 34,87
Buss H.R., Tielens A.G.G.M., Cohen M., et al., 1993, ApJ 415,250
Cesarsky C.J., Abergel A., Agnese P., et al., 1996, A&A 315,L32
Cohen M., Tielens A.G.G.M., Bregman J., et al., 1989, ApJ 341,246
Guerrero M.A., Manchado A., 1997, ApJ 487,328
Hora J.L., Deutsch L.K., Hoffmann W.F., Fazio G.G., Shivanandan K., 1993, ApJ 413,304
Hora J.L., Deutsch L.H., Hoffmann W.F., Fazio G.G., 1996, AJ 112,2064
Kessler M.F., Steinz J.A., Anderegg M.E., et al., 1996 A&A 315,L27
Latter W.B., Kelly D.M., Hora J.L., Deutsch L.K., 1995, ApJS 100,159
Lester D.F., Dinerstein H.L., 1984, ApJ 281,L67
Lucy L.B., 1974, AJ 79,745
Mattila K., Lemke D., Haikala L.K., et al., 1996, A&A 315,L353
Ott S., Abergel A., Altieri, B., et al., 1997, In: Hunt G., Payne H.E. (eds.) Astronomical Data Analysis Software and Systems. ASP Conf.Ser. 125, 34 1997
Persi P., Cesarsky D., Rouan D., Siebenmorgen R., 1997, Proc. First ISO Workshop on Analytical Spectroscopy, ESA SP-419, p. 95
Persi P., Cesarsky D., Marenzi A.R., et al., 1999, Proc. The Universe as seen by ISO, ESA SP-, in press
Pottasch S.R., Preite-Martinez A., Olnon F.M., Jing-Er M., Kingma S., 1986, A&A 161,363
Pottasch S.R., Beintema D.A., 1997, Proc. First ISO Workshop on Analytical Spectroscopy, ESA SP-419, p. 73
Puget J.-L., Leger A., 1989, ARA&A 27,161
Richardson W.H., 1972, J. Opt.Soc.Am. 62, 55
Roche P.F., Aitken D.K., 1986, MNRAS 221,63
Russell R.W., Soifer B.T., Willner, S.P., 1977, ApJ 217,L149
Sahai R., Trauger J.T., 1998, AJ 116,1357
Siebenmorgen R., Krugel E., 1992 A&A 259,614
Siebenmorgen R., Zijlstra A.A., Krugel E., 1994, MNRAS 271,449
Siebenmorgen R., Starck J.L., Cesarsky D.A., Guest S., Sauvage M., 1997, ISOCAM Data Users Manual Version 3.0, ESA document, Reference: SAI/95–222/Dc
Starck J.L., Murtagh F., Pirenne B., Albrecht M., 1996 PASP 108,446
Woodward C.E., Pipher J.L., Shure M., Forrest W.J., Sellgren K., 1989, ApJ 342,860